

CuTi LDH derived NH₃-SCR catalysts with highly dispersed CuO active phase and improved SO₂ resistance

Qinghua Yan¹, Yu Nie¹, Ruoyan Yang¹, Yuhan Cui¹, Dermot O'Hare², Qiang Wang^{1,*}

¹College of Environmental Science and Engineering, Beijing Forestry University, 35
Qinghua East Road, Haidian District, Beijing 100083, P. R. China

²Chemistry Research Laboratory, Department of Chemistry, University of Oxford, 12
Mansfield Road, Oxford, OX1 3TA, UK

*Corresponding author:

College of Environmental Science and Engineering, Beijing Forestry University, 35
Qinghua East Road, Haidian District, Beijing 100083, P. R. China

E-mail: qiang.wang.ox@gmail.com; qiangwang@bjfu.edu.cn

Tel: +86 13699130626

Abstract

For NO_x removal from the exhaust gases of municipal solid waste (MSW) incinerators by selective catalytic reduction (SCR) technology, a suitable SCR catalyst which is active at low temperatures and robust to the presence of alkali metals and SO₂ is highly desired. In this contribution, we report the successful fabrication of a highly dispersed Cu_yAlO_x ($y = 2-4$) mixed oxides for NH₃-SCR catalyst using high surface area, flower-like highly dispersed AMO-Cu-Al-CO₃ LDHs precursors. The influence of the Cu/Al ratio (2, 3, 4, and 5), calcination temperature (400, 500, 600, and 700 °C), and testing temperature (150, 200, 250, and 300 °C) on the activity of the Cu_yAlO_x mixed oxide catalysts were systematically investigated. Among all samples, Cu₄AlO_x showed the highest NO_x conversion of 91.1% at 200 °C. After being thermally treated at 700 °C, the NO_x conversion of Cu₄AlO_x was still as high as 84.7%, which is much higher than that of the control catalyst 10 wt% CuO/γ-Al₂O₃ (57.5%). XRD and HR-TEM analyses suggested that the highly dispersed CuO nanoparticles are the active species for the SCR reaction. The catalytic De-NO_x performance of Cu₄AlO_x in the presence of alkali metals (K and Na) and SO₂ was also studied. In the presence of 50 ppm SO₂, the NO_x conversion of Cu₄AlO_x (78.4%) was much higher than that of CuO/γ-Al₂O₃ (48%). The selectivity of NO_x conversion to N₂ and resistance to H₂O (and co-existence of H₂O and SO₂) for Cu₄AlO_x catalyst were also evaluated. In all, we have demonstrated that the newly obtained Cu₄AlO_x catalyst not only possesses higher thermal stability and higher low temperature (150–250 °C) catalytic activity, but also has much better alkali metal (K and Na), SO₂, and H₂O resistance than a conventional CuO/γ-Al₂O₃ catalyst.

Key words: selective catalytic reduction; municipal solid waste incineration; layered double hydroxides; alkali metals; sulfur dioxide

1. Introduction

For the sustainable development of society, municipal solid waste (MSW) has to be managed to avoid the exclusive use of landfills. Waste incineration is an increasingly used route to get rid of MSW due to the primary advantages of weight reduction, volume reduction, hygienic control, and energy recovery [1]. However, the main problem for the incineration treatment is the release of significant amounts of harmful pollutants, including heavy metals (e.g., Cd, Pb, and Hg), acid gases (e.g., NO_x, CO, SO_x, and HCl), and hydrocarbons [2]. In recent years, with the regulations for NO_x emission becoming more and more stringent, the NO_x abatement technologies for MSW incineration flue gases are receiving more and more attention. In China, for instance, the NO_x emission limit of hourly average was reduced from 400 mg/m³ in GB18485-2001 to 250 mg/m³ in DB11 502-2008. In addition, the actual implemented NO_x emission limit of hourly average for new plants that are under construction in Beijing is even lower, which is 80 mg/m³. With more stringent regulations on NO_x emission from MSW incineration flue gases, efficient and reliable De-NO_x technologies are highly desirable [3].

As the concentration of NO_x emitted from MSW incineration plants is in the similar range as that from coal-fired power plants, selective catalytic reduction (SCR) technology has been systematically investigated because of its good selectivity, high efficiency, low cost, and is currently applied in MSW incineration plants in some countries such as Japan, Denmark, and Sweden [4]. The mostly adopted SCR catalysts for practical applications are V₂O₅-MoO₃/TiO₂ and V₂O₅-WO₃/TiO₂, with an active temperature range of 300–400 °C [5, 6]. However, for the MSW incineration flue gases, because the concentration of SO₂ is normally very high, the SCR unit is preferred to be placed in downstream of the desulfurizer. For such configuration, the temperature of the exhaust gases is much lower and the vanadium-based

high-temperature SCR catalysts do not work properly under this condition [7-10]. Reheating the exhaust gases is not economical. In addition, the vanadium-based SCR catalysts also suffer from the poisoning effects by other harmful pollutants such as alkali metals and SO₂ that exit in the MSW flue gases [11, 12]. Thus, developing novel SCR catalysts that are highly active at relatively lower temperatures and are resistant to alkali metals and SO₂ is of great importance for NO_x emission control from MSW flue gases.

To date, several types of low-temperature NH₃-SCR catalysts have been reported, including noble metals-based [13], zeolite-based [14, 15], MnO_x-based [16], and CuO-based catalysts [17, 18]. Among these catalysts, noble metals-based catalysts are expensive while zeolite-based catalysts have relatively poor stability in the presence of HCl [19-21]. MnO_x-based catalysts have good activity but suffer from SO₂ poisoning [22, 23]. Comparing to other catalysts, CuO catalysts supported on various supports, such as CuO/ZrO₂ [24-26], CuO/γ-Al₂O₃ [27], CuO/SiO₂ [28] and CuO/TiO₂ [29, 30] showed good NH₃-SCR activities. It was believed that the activity and selectivity of CuO-based catalysts are highly dependent on the texture and dispersion state of CuO species, which are importantly influenced by the preparation method [31]. In addition, for the supported CuO catalysts, the active CuO is often associated with sintering and aggregation when being exposed to high temperatures, leading to reduced SCR activity.

Recently, the synthesis of highly dispersed mixed metal oxides based catalysts via the careful calcination of a highly dispersed layered double hydroxide (AMO-LDH) precursors has attracted great attention [32-34]. Using this approach the dispersion of active metal species can be controlled at the atomic level [35-39]. Inspired by these studies, we now report the successful preparation of novel highly

dispersed Cu_yAlO_x ($y = 2-4$) mixed oxides as NH_3 -SCR catalysts from AMO-Cu-Al- CO_3 LDHs. Due to the better dispersion of active CuO species, these Cu_yAlO_x mixed oxide catalysts showed much higher De- NO_x activity and better resistance to alkali metals and SO_2 than those of the supported $\text{CuO}/\gamma\text{-Al}_2\text{O}_3$ catalyst. The influences of Cu/Al ratio, calcination temperature and reaction temperatures were systematically investigated. In addition, the poisoning effects of alkali metals and SO_2 on the surface acidity and reducibility were evaluated.

2. Experimental

2.1. Preparation of highly dispersed Cu_yAlO_x ($y = 2-5$) mixed oxide catalysts

First, conventional Cu-Al- CO_3 LDHs, $[\text{Cu}_{1-x}\text{Al}_x(\text{OH})_2]_x(\text{CO}_3)_{x/2}$ were synthesized via a standard co-precipitation method. For instance, for the synthesis of $\text{Cu}_2\text{Al-}\text{CO}_3$ LDH, $\{[\text{Cu}_{0.66}\text{Al}_{0.33}(\text{OH})_2](\text{CO}_3)_{0.165}\}$ an 100 mL aqueous solution containing 0.025 mol $\text{Al}(\text{NO}_3)_3 \cdot 9\text{H}_2\text{O}$ and 0.05 mol $\text{Cu}(\text{NO}_3)_2 \cdot 6\text{H}_2\text{O}$ and was added drop-wise into a vigorously stirred basic solution (100 mL) including 0.05 mol Na_2CO_3 . During the synthesis, the pH of solution were maintained at 10 by addition of a NaOH solution (4 M). The slurry was stirred continuously for another 12 h. After aging, the resulting precipitate was filtered, washed several times with deionized water until $\text{pH} = 7$. The damp solids were then exposed to the Aqueous Miscible Solvent Treatment Method (AMOST), which involved washing and stirred for 2 h with acetone to give highly dispersed AMO-Cu-Al- CO_3 LDHs [32-34]. Finally, the AMO- $\text{Cu}_2\text{Al-}\text{CO}_3$ LDH was obtained by drying at 60 °C in the oven for another 24 h. Similarly other AMO-Cu-Al- CO_3 LDHs with different Cu/Al ratios of 3, 4, and 5 can be prepared by simply changing the $\text{Cu}(\text{NO}_3)_2 \cdot 6\text{H}_2\text{O}$ amount. After being calcined at different temperatures (400–700 °C), various Cu_yAlO_x mixed oxides were obtained, which

were denoted as Cu_2AlO_x , Cu_3AlO_x , Cu_4AlO_x , and Cu_5AlO_x , respectively.

The conventional supported catalyst 10 wt% $\text{CuO}/\gamma\text{-Al}_2\text{O}_3$ was prepared by incipient wetness impregnation method with an aqueous solution of $\text{Cu}(\text{NO}_3)_2 \cdot 6\text{H}_2\text{O}$. After being dried at 60 °C in the oven for 12 h, the samples were calcined at different temperatures (400–700 °C) in air for 5 h.

2.2 Characterization of catalysts

The X-ray diffraction (XRD) patterns of all synthesized samples were characterized using a Shimadzu XRD-7000 instrument in reflection mode with Cu $K\alpha$ radiation ($\lambda = 1.542 \text{ \AA}$). The accelerating voltage was set at 40 kV with 30 mA current. Diffraction patterns were recorded within the 2θ range of 5–70° with the setting scan speed of 5 °/min and a step size of 0.02°. The morphology of samples was characterized using field emission scanning electron microscope (FE-SEM, SU-8010, Hitachi). High resolution transmission electron microscopy (HR-TEM) analyses were performed on JEM-2100 microscope (JEOL, Japan) with an accelerating voltage of 200 kV. Fourier transform infrared spectrometer (FT-IR) experiments were performed on a FTS 3000 MX FT-IR (Bruker Vertex 70) spectrophotometer. BET specific surface areas (SSA) of samples were measured with a physisorption analyser (SSA-7000, Builder). The calcined Cu_yAlO_x mixed oxides samples were degassed at 220 °C for 4 h. Thermogravimetric analyses (TGA) of samples were conducted on a Q50 TGA analyzer from the TA Instruments. The samples were loaded onto the sample holder, and the temperature of the TGA furnace was increased to 800 °C in a flowing air (60 ml/min) with a rate of 5 °C/min.

The surface acidity of Cu_yAlO_x mixed oxides catalysts was measured by temperature-programmed desorption of ammonia (NH_3 -TPD) in a fixed-bed continuous flow microreactor system. The desorbed molecules were monitored

on-line using a quadrupole mass spectrometer (QGA, Hidden, UK). Before NH₃-TPD measurement, the catalyst (0.15 g) was purged in a flow of pure Ar at 400 °C for 30 min. Then, the furnace temperature was cooled down to 100 °C, and the samples were saturated in a flow of 1% NH₃/Ar (40 ml/min) for about 1 h. Subsequently, the sample was purged in Ar to remove weakly bound (physisorbed) NH₃, until a stable baseline level was achieved. TPD of ammonia was detected from 100 to 600 °C in a flow of Ar (40 ml/min) with a linear heating rate of 2 °C/min. The temperature in the catalyst bed was controlled using a K-type thermocouple immersed in the catalyst bed. The temperature-programmed reduction (TPR) of samples was detected from 100 to 600 °C in a fixed-bed flow microreactor (10 mm internal diameter). The hydrogen consumption was monitored using a quadrupole mass spectrometer (QGA, Hidden, UK). Prior to the TPR experiment, the sample (0.15 g) was purged in a flow of pure Ar at 400 °C for 30 min until a stable baseline level was achieved. Then, the furnace temperature was cooled down to 100 °C. The TPR runs were carried out in a flow of 5% H₂ in Ar (100 ml/min) with a linear heating rate of 2 °C /min.

2.3 NH₃-SCR activity tests

The NH₃-SCR catalytic activities of synthesized catalysts were performed at atmospheric pressure in a fixed-bed stainless steel reactor with an internal diameter of 10 mm. For each test, 0.15 g of catalyst was charged. After the reactor was heated up to the desired reaction temperature, the gas mixture was fed to the reactor. The reaction gas mixture normally consisted of 500 ppm NO_x, 500 ppm NH₃, 5% O₂, and Ar in balance, with a flow rate of 200 mL/min. All the gas flows were controlled independently by mass flow controllers (Brooks Instruments). The change of NO_x concentration was continuously measured using an on-line NO_x analyzer (Thermo Scientific 42i-HL, USA). The NO_x (NO and NO₂) conversion was calculated using the

follow equation (1). The N₂ selectivity was evaluated using a quadrupole mass spectrometer (QGA, Hidden, UK). The simulated flue gas was composed of 500 ppm NO_x, 500 ppm NH₃, 5% O₂, and Ar as the balance gas.

$$NOx \text{ conversion} = \left(1 - \frac{NOx(out)}{NOx(in)} \right) \times 100\% \quad (1)$$

2.4 Poisoning and regeneration of catalysts

The alkali metals doping of Cu_yAlO_x mixed oxides and CuO/γ-Al₂O₃ catalysts were prepared by impregnating with KNO₃ and NaNO₃ solutions. After being dried at 60 °C for 12 h, the nitrates were decomposed at 400 °C for 5 h in flowing air. Both Cu_yAlO_x mixed oxides and CuO/γ-Al₂O₃ catalysts were poisoned with an equal mass loading of K and Na of 0.25 wt% or 0.5 wt%. The catalysts after loading K and Na were denoted as PK or PNa. The regeneration of alkali metal poisoned catalysts was performed by washing the catalyst with 100 ml deionized-water under continuous stirring for 1 h, and followed by drying at 60 °C in the oven for 12 h. Then, the samples were calcined at 400 °C in air for 5 h. The correspondingly regenerated catalysts were denoted as dK and dNa, respectively.

The poisoning effect of SO₂ on the activity of Cu_yAlO_x mixed oxide catalysts was studied by introducing 50 or 100 ppm SO₂ to the inlet gas (500 ppm NO_x, 500 ppm NH₃, 5% O₂, 50 or 100 ppm SO₂, balance Ar). The thermal stability of the formed sulfate species was evaluated using temperature programmed desorption, and the desorbed SO₂ was monitored using a quadrupole mass spectrometer (QGA, Hidden, UK). The regeneration of sulfated catalysts was performed by thermal treatment at 400 °C for 1 h in Ar flow.

The poisoning of H₂O was studied by introducing 5% H₂O to the inlet gas (500

ppm NO_x, 500 ppm NH₃, 5% O₂, balance Ar). Liquid water was continuously added using a syringe pump (Lead fluid, TYD01) into a stainless steel tube wrapped with a temperature-controlled heating tape, in which water vapor was generated. The change of NO_x concentration was continuously measured using an on-line NO_x analyzer (Thermo Scientific 42i-HL, USA).

3. Results and discussion

3.1 Characterization of AMO-Cu-Al-CO₃ LDHs

The XRD patterns of synthesized AMO-Cu-Al-CO₃ LDHs {[Cu_{1-x}Al_x(OH)₂]_x(CO₃)_{x/2}} with different Cu/Al molar ratios (Cu/Al = 2, 3, 4 and 5) were first characterized using XRD analysis, as shown in Fig. 1(a). In the XRDs sharp and intense Bragg reflections are observed in 2θ range 5–70°. The Bragg reflections at 2θ = 11.73°, 23.76°, 34.74°, 39.76°, and 47.86°, may be indexed to the (003), (006), (009), (015), and (018) reflections of a standard LDHs unit cell (JCPDS no. 46-0099), respectively [40]. Due to the Jahn–Teller distortion of the Cu²⁺ ions in the octahedral coordination sites within the layered structure of Cu-Al-CO₃ LDH the formation of a small CuO impurity cannot be prevented [41]. Figure 1(a) contains some weak Bragg reflections due to CuO at 2θ = 32.5°, 35.5°, and 38.73°, which correspond to the reflections of (–110), (–111), and (111) planes of CuO (JCPDS no. 45-0937), respectively.

The FT-IR spectra of AMO-Cu-Al-CO₃ LDH nanoparticles is shown in Fig. 1(b). A broad absorption band centered at 3450 cm^{–1} is attributed to stretching vibrations of –OH groups in the brucite-like layers, the lattice water and the interlayer water molecules [42–44]. The vibration of angular deformation of H₂O molecules is observed at 1550 cm^{–1} [45]. The absorption at 1356 cm^{–1} in the spectrum is attributed to the vibrations of carbonate ions. Finally, the absorption bands around 604 and 443

cm^{-1} are attributed to the vibrations of the M–O (M–OH, M–O–M or O–M–O) [44, 46, 47]. Both XRD and FTIR data confirmed the successful synthesis of AMO-Cu-Al- CO_3 LDHs with different Cu/Al molar ratios.

The morphology of synthesized AMO-Cu-Al- CO_3 LDHs were examined using FE-SEM and TEM analyses. All LDHs formed similar “flower-like” morphology to that of AMO-Cu₄Al- CO_3 LDH, as shown Fig. 1(c). The flower-like particles are composed of well-defined nanoplatelets. The “flower-like” morphology was further confirmed by the TEM image in Fig. 1(d), which indicates that the LDHs nanoplatelets were very thin. It also shows that the nanoparticles are highly porous, which is favorable for the gas-solid heterogeneous catalytic reactions. The AMO-Cu-Al- CO_3 LDHs were then calcined between 400–700 °C to give highly dispersed Cu_yAlO_x mixed oxides, the XRD patterns of which are shown in Fig. 2(a). For the 400 °C calcined sample, the broad Bragg reflections are observed that may be attributed to nano-CuO particles. Using the Scherrer equation we can estimate these particles to have a crystallite domain size of ca. 8.93 nm. On further heating at higher temperatures, these reflections became sharpen as the particles were further crystallised. And in the meantime, some new reflections due to the spinel phase CuAl_2O_4 were observed. The specific surface areas (SSA) of Cu_yAlO_x ($y = 2\text{--}5$) samples were measured using BET analysis method, which are in the range of 93–108 m^2/g (Table 1).

3.2 SCR activity of Cu_yAlO_x mixed oxide catalysts

For the Cu-based SCR catalysts, it is apparent that the Cu/Al ratio will have a significant effect on the activity. In addition, for LDHs-derived mixed oxide catalysts, calcination temperature is another important parameter that affects the generation of

active phase, and has obvious effects on various characteristics such as specific surface area, pore volume, and pore size, etc. Therefore, the influences of Cu/Al ratio and calcination temperature on the activity of Cu_yAlO_x mixed oxide catalysts were first evaluated at different operating temperatures (150–300 °C). Fig. 3 shows that the Cu/Al ratio has obvious effect on the catalytic performance of Cu_yAlO_x mixed oxide catalysts. The NO_x conversion first increased with the increase in Cu/Al ratio from 2 to 4, and then started to decrease when the Cu/Al ratio was 5. Under all testing conditions, Cu_4AlO_x catalyst resulted in the highest NO_x conversion. For instance, for the samples calcined at 400 °C, the NO_x conversion was 86.7%, 88.4%, 91.1%, and 79.3% for Cu_2AlO_x , Cu_3AlO_x , Cu_4AlO_x , and Cu_5AlO_x , respectively.

In order to show the advantages of AMO treatment, a control $\text{Cu}_4\text{Al-CO}_3$ LDH without AMO treatment was also prepared by water washing only. By thermal treatment of this water washed $\text{Cu}_4\text{Al-CO}_3$ LDH at 400 °C, a control catalyst Cu_4AlO_x (W) was then obtained. Activity tests indicates that the NO_x conversion of Cu_4AlO_x (W) was only 71.0% at 200 °C, which is much lower than that of Cu_4AlO_x obtained with AMO treatment (91.1%). This data clearly suggests that the AMO treatment is crucial for the high catalytic activity of Cu_yAlO_x . For this reason, all the following Cu_yAlO_x ($y = 2-4$) catalysts used in this work were prepared from AMO-Cu-Al- CO_3 precursor.

One advantage of Cu_yAlO_x mixed oxide catalysts is that they are highly thermally stable. With the increase in calcination temperature from 400 to 700 °C, the catalytic activity only slightly decreased. For instance, for the Cu_4AlO_x catalyst that was calcined at 400, 500, 600, and 700 °C, the NO_x conversion at 200 °C were 91.1%, 89.3%, 88.2%, and 84.7%, respectively. The NO_x conversion drop is only 6.4% even after being calcined at 700 °C for 5 h, suggesting that the Cu_4AlO_x catalyst is sintering

resistant. This property is very important as the operating temperature might occasionally rise to quite high. In addition, the regeneration of sulfated catalysts also requires high-temperature treatment. In order to study the selectivity of Cu_4AlO_x catalyst for NO_x conversion to N_2 , the productions of N_2O and N_2 during the SCR reaction at 200 °C were monitored, as shown in Fig. 5(a). It is clear that only negligible amount of N_2O was observed. While in contrast, the production of N_2 was very significant. The result indicated that the Cu_4AlO_x catalyst not only possesses high catalytic conversion, but also high selectivity to N_2 . In all, it can be concluded that the 400 °C-calcined Cu_4AlO_x sample was the best NH_3 -SCR catalyst for the reduction of NO_x . Fig. 3 also indicates that the Cu_4AlO_x catalyst is active at relatively low temperatures and 200 °C was the optimal operating temperature.

After revealing the best catalyst candidate, the impact of catalyst amount (0.1, 0.15, and 0.2 g) was studied, as shown in Fig. S1. When using 0.1 g catalyst, the NO_x conversion was only 77.6%. By increasing the catalyst amount to 0.15 g, the NO_x conversion was significantly increased to 91.1%. However, by further increasing the catalyst amount to 0.2, negligible improvement was obtained in the NO_x conversion (91.9%). From the perspective of the utilization efficiency of catalyst, 0.15 g was chosen as the best catalyst amount for all the following catalytic evaluations.

3.3 Comparison of Cu_4AlO_x and $\text{CuO}/\gamma\text{-Al}_2\text{O}_3$ catalysts

Previously, there are a few reports on conventional supported $\text{CuO}/\text{Al}_2\text{O}_3$ as NH_3 -SCR catalyst. For instance, in 1995, Centi et al. [48, 49] systematically investigated the influence of reaction temperature and the CuO loading on the NO_x conversion of $\text{CuO}/\text{Al}_2\text{O}_3$ catalysts. It was found that with 10 wt% of CuO loading, a 90% of NO_x conversion was achieved at 300 °C. However, its activity at lower

operating temperature range ($<250\text{ }^{\circ}\text{C}$) was not so high. For instance, a NO_x conversion of only ca. 67% was obtained at $250\text{ }^{\circ}\text{C}$. Later on, Suárez et al. [27] studied the performance of a $\text{CuO}/\text{Al}_2\text{O}_3$ monolith catalyst, and found that the best CuO loading was 6.4 wt%, with a NO_x conversion of only 75% at $200\text{ }^{\circ}\text{C}$. The NO_x conversion started to decrease with the increasing of CuO loading, suggesting that the low-temperature NH_3 -SCR activity of conventional supported $\text{CuO}/\text{Al}_2\text{O}_3$ catalyst can not be improved by simply increasing the CuO loading. Thus, up to date, the conventional $\text{CuO}/\text{Al}_2\text{O}_3$ catalyst generally failed to deliver good performance at low temperature range ($<250\text{ }^{\circ}\text{C}$). However, the new catalyst Cu_4AlO_x that we synthesized from $\text{Cu}_4\text{Al-CO}_3$ LDH can lead to a much higher NO_x conversion of 91.1% at $200\text{ }^{\circ}\text{C}$. This data suggests that this new catalyst Cu_4AlO_x is very much different from the conventional supported $\text{CuO}/\text{Al}_2\text{O}_3$ catalyst and is much superior for low-temperature NH_3 -SCR reaction.

In order to further confirm the above conclusion, the performance of the newly prepared, high dispersed Cu_4AlO_x catalyst was compared with a control catalyst $\text{CuO}/\gamma\text{-Al}_2\text{O}_3$ by using different calcination temperatures ($400\text{--}700\text{ }^{\circ}\text{C}$) and different operating temperatures ($150, 200, 250$, and $300\text{ }^{\circ}\text{C}$). Fig. 4 indicates that the catalytic activity of Cu_4AlO_x is much higher than that of $\text{CuO}/\gamma\text{-Al}_2\text{O}_3$ under all different conditions. For instance, after being calcined at $400\text{ }^{\circ}\text{C}$, the maximum NO_x conversion of Cu_4AlO_x was 91.1%, higher than that of $\text{CuO}/\gamma\text{-Al}_2\text{O}_3$ (82.5%). The optimal operating temperature of Cu_4AlO_x ($200\text{ }^{\circ}\text{C}$) was also lower than that of $\text{CuO}/\gamma\text{-Al}_2\text{O}_3$ ($250\text{ }^{\circ}\text{C}$), suggesting Cu_4AlO_x is more preferable than $\text{CuO}/\gamma\text{-Al}_2\text{O}_3$ to serve as low-temperature SCR catalyst. In addition, the catalytic activity of $\text{CuO}/\gamma\text{-Al}_2\text{O}_3$ at $200\text{ }^{\circ}\text{C}$ decreased significantly with the increase in calcination temperature. For instance, after being calcined at $700\text{ }^{\circ}\text{C}$, the NO_x conversion at $200\text{ }^{\circ}\text{C}$ dropped

significantly to 57.5%. However, for Cu_4AlO_x catalyst, the NO_x conversion at 200 °C was still as high as 84.7% after calcination at 700 °C.

In order to understand why the Cu_4AlO_x catalyst is more sintering resistant than $\text{CuO}/\gamma\text{-Al}_2\text{O}_3$, the XRD patterns of these two catalysts were examined after being calcined at different temperatures. Fig. 2(a) shows the XRD patterns of Cu_4AlO_x calcined at 400, 500, 600, and 700 °C, respectively. When the calcination temperature was lower than 600 °C, only CuO was detected, and the intensity of the peaks increased with the increase in calcination temperature, suggesting that the particle size increased after being calcined at higher temperatures. At 700 °C, in addition to the CuO as the major phase, some weak peaks corresponding to CuAl_2O_4 spinel start to be observed. In addition, Cu_4AlO_x remained its “flower-like” morphology after being calcined at 400 °C, which is similar to its precursor AMO- $\text{Cu}_4\text{Al-CO}_3$ LDH, as shown Fig. 2(b). However, for the $\text{CuO}/\gamma\text{-Al}_2\text{O}_3$ catalyst, the Cu mainly presented as CuAl_2O_4 spinel (Fig. 5(b)). When the calcination temperature is no more than 400 °C, some weak peaks corresponding to CuO phase was detected. This data suggested that the highly dispersed CuO species may be more likely to promote the conversion of NO_x into N_2 than CuAl_2O_4 spinel at low temperatures, and the activity of difference Cu_4AlO_x and $\text{CuO}/\gamma\text{-Al}_2\text{O}_3$ is less affected by the morphology of the catalysts.

Besides the structural changes during thermal treatment, the memory effect (structure reconstruction) of AMO- $\text{Cu}_4\text{Al-CO}_3$ LDH was also taken into consideration. After AMO- $\text{Cu}_4\text{Al-CO}_3$ LDH was calcined at 400 °C, it was exposed to air for 6 days. The structure of the samples were examined by XRD once a day. Figure 5(c) shows that Cu_4AlO_x still did not change back to their original layered structure even after 6 days.

In order to further confirm the “memory effect” performance of AMO-Cu₄Al-CO₃ LDH, FT-IR analysis was also carried out on calcined Cu₄AlO_x, as shown in Fig. S2. The data further confirmed that Cu₄AlO_x still did not change back to their original layered structure. This sample was further evaluated and resulted in a NO_x conversion as high as 90.8% at 200 °C. This result clearly demonstrated that our developed Cu₄AlO_x is not affected by the memory effect.

In order to have a clearly understanding on how the catalytic activities of Cu₄AlO_x and CuO/γ-Al₂O₃ were influenced by calcination temperature, we further analyzed the data obtained from X-ray diffraction patterns using a normalized relative intensity ratio (RIR) method given by equation 2 [50, 51], which was aimed to investigate the influence of CuO phase amount on the NO_x conversion capacity of samples from the viewpoint of crystalline phase abundance. In this equation, x means one phase in the all definite crystalline phases of analyzed sample and W_x represents the phase abundance of x phase. A is representative for the phase selected to work as an internal standard, and I_x denoted the intensity of a specific pattern of x phase which can be obtained from the peak report using Jade analysis software. What's more, K_A^x will be calculated by the following equation 3. In this equation, K_x is equal to the RIR value of x phase, which can be referred at the relevant PDF card.

$$W_x = \left(\frac{K_A^x}{I_x} \sum_{i=A}^n \frac{I_i}{K_A^i} \right)^{-1} \quad (2)$$

$$K_A^x = \frac{K_x}{K_A} \quad (3)$$

The molar percentages of CuO and CuAl₂O₃ phases in both Cu₄AlO_x and CuO/γ-Al₂O₃ samples calcined at different temperatures were calculated using the above mentioned RIR method, as summarized in Table 2. With the increase in

calcination temperature, the amount of CuO species in Cu_4AlO_x and $\text{CuO}/\gamma\text{-Al}_2\text{O}_3$ started to decrease from 400 °C. For the Cu_4AlO_x samples calcined at 400, 500, 600, and 700 °C, the mole percentage of CuO was 100%, 99.2%, 97.5%, and 94.9%, respectively. For a comparison, there was only around 58% CuO phase in the $\text{CuO}/\gamma\text{-Al}_2\text{O}_3$ calcined at 400 °C. With increasing the calcination temperature to 500, 600, and 700 °C, the molar percentage of CuO phase further decreased to 54%, 40.8%, and 27.7%, respectively. The variation in relative molar fraction of CuO followed the same trend to the catalytic activity, indicating that the amount of active CuO species is crucial for NO_x conversion.

Fig. 6 shows the HR-TEM images of Cu_4AlO_x and $\text{CuO}/\gamma\text{-Al}_2\text{O}_3$ catalysts. For the Cu_4AlO_x catalyst, well dispersed CuO nanoparticles with an average particle size of ~10 nm were observed. A lattice fringe with a spacing distance of 0.25 nm was observed in Fig. 6(c), which can be referenced to the (-111) crystal plane of CuO. While for the $\text{CuO}/\gamma\text{-Al}_2\text{O}_3$ catalyst, few CuAl_2O_4 nanoparticles with an average particle size of ~20 nm were seen. This data suggest that the synthesis of SCR catalysts from AMO-Cu-Al- CO_3 LDHs precursors can lead to the formation of highly dispersed and nano-sized CuO species. In addition, the valence state of Cu in Cu_4AlO_x catalyst was examined using XPS analysis, as shown in Fig. 7. It can be seen from the XPS spectrum of Cu 2p_{3/2} that two peaks are discerned at 934.2 and 932.9 eV. The higher binding energy peak at 934.2 eV is assigned to Cu^{2+} , accompanied by the characteristic Cu^{2+} shake-up satellite peaks [52]. The lower binding energy peak at 932.9 eV suggests the presence of Cu^+ species. The relative concentration of Cu^{2+} is 86.7%, which indicates that Cu^{2+} is the majority state in Cu_4AlO_x catalyst. The XPS result is also consistent with the results of XRD and HR-TEM, indicating that the copper is mainly in the form of CuO, which is highly dispersed in Cu_4AlO_x catalyst.

The high dispersed CuO species in Cu₄AlO_x catalyst is advantageous to the catalytic reaction comparing to the CuAl₂O₄ species in CuO/ γ -Al₂O₃ catalyst, particularly at low temperatures.

3.4 The alkali metals poisoning and regeneration of catalysts

Fine fly ash has been a major concern to SCR catalysts. Fly ash may plug the pores of catalyst and react with the active phases [53]. Alkali oxides and/or salts are major components in fly ash and have strongly poison on the SCR catalysts [54, 55]. In order to research the poisoning effect of alkali metals on this newly developed Cu₄AlO_x catalysts, poisoned catalysts were prepared by doping 0.25 wt% (or 0.5 wt%) K or Na onto the catalysts. The NO_x conversions of fresh and alkali metals poisoned catalysts are compared in Fig. 8(a). For both 0.25 wt% K and Na-doped Cu₄AlO_x catalysts, the NO_x conversions decreased from 91.1% for fresh catalyst to 74.3% and 74.7%, respectively, indicating that K and Na have similar poisoning effect on Cu₄AlO_x. With increasing the K or Na loading to 0.5 wt%, the NO_x conversion of Cu₄AlO_x catalyst further decreased to 60.4% and 65.1%, respectively. For comparison purpose, the poisoning effect of alkali metals on CuO/ γ -Al₂O₃ catalyst was also performed. Similarly, the NO_x conversions of 0.25 wt% K and Na-doped CuO/ γ -Al₂O₃ catalysts also decreased, from 81.8% for fresh catalyst to 68.6% and 69.3%, respectively. With increasing the alkali metals loading (0.5 wt% K or Na), the NO_x conversion of CuO/ γ -Al₂O₃ catalyst significantly decreased to 48.9% and 57%, respectively, which might be because more pores and active phases were occupied by alkali metals. The NO_x conversions of K and Na-doped catalysts dropped to 60.4% and 65.1% for Cu₄AlO_x, for CuO/ γ -Al₂O₃. These results indicate that although the Cu₄AlO_x catalyst could be poisoned to some extent by both K and Na, the poisoned

samples still showed much higher NO_x conversions than those of poisoned CuO/γ-Al₂O₃ catalysts.

In order to solve the poisoning problem caused by alkali metals, the regeneration of the poisoned catalysts is also very important. Shen et al. [56, 57] previously reported that washing with water or sulfuric acid solution could partially recover the SCR activity of poisoned catalysts. And washing with water is believed to be the best method as it will not cause any loss of active species of catalysts. Thus, in this contribution, the regeneration of poisoned Cu₄AlO_x and CuO/γ-Al₂O₃ catalysts was performed by washing with deionized-water and followed by drying at 60 °C for 12 h. Fig. 8(b) shows that the activities of both regenerated catalysts were partially restored. After regeneration, the NO_x conversion of 0.25 wt% K and Na-poisoned CuO/γ-Al₂O₃ was improved from 68.6% and 69.3% to 72.7% and 72.9%, respectively. For the Cu₄AlO_x catalyst, the regenerated samples showed higher NO_x conversions, which were 77.9% and 79.9% for the 0.25 wt% K and Na poisoned Cu₄AlO_x catalysts. Comparing to fresh catalysts, the activity of the regenerated catalysts have a certain degree of decline, which might be the loss of active component during the regeneration process.

It has been established that the surface acidity of catalysts plays an important role in selective catalytic reduction of NO_x by NH₃. One of the most important steps for SCR is the adsorption of NH₃ on catalyst surface. Hence, NH₃-TPD experiments were carried out to investigate the deactivation of catalysts caused by alkali metals. Fig. 9(a) shows the NH₃-TPD curves of the fresh, and 0.25 wt% K and Na-poisoned Cu₄AlO_x catalyst in the temperature range of 100–600 °C. All curves exhibit one NH₃ desorption peak at around 157–201 °C, which can be attributed to Lewis acid sites[58]. The amount of Lewis acid sites can be roughly estimated from the area of NH₃-TPD

peak. For Cu_4AlO_x catalyst, the NH_3 -TPD peaks did not change much after 0.25 wt% K and Na poisoning, suggesting that neither K nor Na had much effect on the amount of Lewis acid sites. However, the peak temperature slightly shifted to higher temperatures after being poisoned by K (186 °C), and Na (201 °C), suggesting that the interaction between Lewis acid sites and adsorbed NH_3 became stronger. The slight activity decrease for the 0.25 wt% K and Na poisoned Cu_4AlO_x catalysts might be explained by the fact that the surface acid sites became stronger. Lisi et al. [4] reported that strong acid sites adsorbing ammonia at $T > 350$ °C are not involved in the low-temperature SCR reactions. However, in the case of $\text{CuO}/\gamma\text{-Al}_2\text{O}_3$ catalyst, 0.25 wt% K and Na significantly reduced the amount of surface Lewis acid sites, with the NH_3 -TPD peaks obviously weakened (Fig. 9(b)). The amount of acid sites of samples follows the sequence of Cu_4AlO_x (1.33 mmol/g) > $\text{CuO}/\gamma\text{-Al}_2\text{O}_3$ (1.18 mmol/g) > 0.25 wt% Na- Cu_4AlO_x (0.97 mmol/g) > 0.25 wt% K- Cu_4AlO_x (0.78 mmol/g) > 0.25 wt% Na- $\text{CuO}/\gamma\text{-Al}_2\text{O}_3$ (0.67 mmol/g) > 0.25 wt% K- $\text{CuO}/\gamma\text{-Al}_2\text{O}_3$ (0.2 mmol/g). This sequence agreed well with the trend of NO_x removal efficiencies as presented in Fig. 8(b). The results indicate that the Lewis acid sites on $\text{CuO}/\gamma\text{-Al}_2\text{O}_3$ catalyst could be neutralized by the doped K^+ and Na^+ ions, leading to decreased amount of surface weak acid sites and thus remarkable decrease of SCR activity. In all, it can be concluded that the surface Lewis acid sites of Cu_4AlO_x catalyst were less effected by K and Na poisoning than that of $\text{CuO}/\gamma\text{-Al}_2\text{O}_3$ catalyst.

The surface redox property is another important property for SCR catalysts. Fig. 9(c, d) show the H_2 -TPR profiles of fresh and poisoned Cu_4AlO_x and $\text{CuO}/\gamma\text{-Al}_2\text{O}_3$ catalysts. For Cu_4AlO_x catalyst, there is only one low-temperature (216–299 °C) reduction peak for both fresh and poisoned Cu_4AlO_x sample (Fig. 9(c)), which can be assigned to the highly dispersed CuO species that are relatively easier to be reduced,

i.e., $\text{Cu}^{2+} \rightarrow \text{Cu}^+ \rightarrow \text{Cu}$ [59]. However, $\text{CuO}/\gamma\text{-Al}_2\text{O}_3$ displayed two reduction peaks with one located between 170–184 °C, and the other at about 360–486 °C in Fig. 9(d). The former can be assigned to the highly dispersed CuO species and the latter can be attributed to the reduction of CuAl_2O_4 spinel [60]. Comparing to $\text{CuO}/\gamma\text{-Al}_2\text{O}_3$, Cu_4AlO_x possesses much stronger low-temperature H_2 -TPR peak, suggesting it has more surface highly dispersed CuO species, which are favorable for the redox reaction. This might be the reason why Cu_4AlO_x catalyst has a higher SCR activity than $\text{CuO}/\gamma\text{-Al}_2\text{O}_3$ catalyst.

After being poisoned by 0.25 wt% K and Na, the intensity of H_2 -TPD peaks of Cu_4AlO_x catalyst did not change much, with the peak temperatures shifted to higher values. This data suggests that although the amount of the active CuO species did not reduce, the redox ability became slightly more difficult. However, for the 0.25 wt% K and Na poisoned $\text{CuO}/\gamma\text{-Al}_2\text{O}_3$ catalyst, the intensity of both low-temperature and high-temperature H_2 -TPR peaks were significantly weakened, and the peak temperatures also shifted to higher values. In all, it can be concluded that the redox property of Cu_4AlO_x was much less effected by the 0.25 wt% K and Na poisoning than that of $\text{CuO}/\gamma\text{-Al}_2\text{O}_3$. It is also noteworthy that the sequence of the amounts of highly dispersed CuO species in different catalysts is in good agreement with that of their catalytic performances.

3.5 SO_2 poisoning and regeneration of catalysts

As there is still certain amount of residual SO_2 in flue gases, the poisoning effect of SO_2 on this newly developed Cu_4AlO_x catalyst was also studied and compared with $\text{CuO}/\gamma\text{-Al}_2\text{O}_3$. In this contribution, 50 or 100 ppm of SO_2 was added to the simulated flue gases for this purpose. The data in the inset of Fig. 10(a) shows that after adding

50 ppm SO₂, the NO_x conversion of Cu₄AlO_x catalyst decreased from 91.1% to 78.4% at 200 °C. However, in the same condition, the decrease in NO_x conversion for CuO/γ-Al₂O₃ was much more obvious, from 81.8% to 48% at 200 °C. In addition, under a high SO₂ concentration (100 ppm) at 200 °C, the NO_x conversions of Cu₄AlO_x still maintained as high as 62.2%, which is also much higher than that of CuO/γ-Al₂O₃ (38.4%) after 6 h reaction. These data clearly demonstrated that the Cu₄AlO_x catalyst possesses a much better resistance to SO₂ than that of CuO/γ-Al₂O₃ at 200 °C. In addition, the effects of 50 ppm SO₂ on the activity of Cu₄AlO_x catalyst at different testing temperatures were also evaluated (Figure S3), which indicated that the Cu₄AlO_x catalyst possesses a much better resistance to SO₂ than that of CuO/γ-Al₂O₃. It is probably because Cu₄AlO_x has more surface highly dispersed copper species than that of CuO/γ-Al₂O₃ catalyst, which could enhance the durability to SO₂ poisoning.

The long-term isothermal NO_x conversions of Cu₄AlO_x and CuO/γ-Al₂O₃ catalysts in the presence of 50 ppm SO₂ at 200 °C was also presented in Fig. 10(b). After running for 6 h, the NO_x conversion of Cu₄AlO_x catalyst only decreased by 5%. However, the decrease in NO_x conversion for CuO/γ-Al₂O₃ was much significant, which is 12% after 6 h running in the presence of 50 ppm SO₂. This isothermal tests also suggested that Cu₄AlO_x catalyst is less influenced by SO₂ than CuO/γ-Al₂O₃.

The deactivation of SCR catalysts caused by SO₂ has been well studied previously [61]. At first, SO₂ could react with NH₃ to form (NH₄)₂SO₃ and NH₄HSO₄, which did not decompose below 200 °C and finally deposited on the catalyst surface, causing pore plugging of catalysts. Secondly, SO₂ may react with the active components such as CuO and form stable sulfate species, which was inactivation for the NH₃-SCR reaction [62]. To clarify the deactivation of SO₂, the SO₂-TPD experiments for Cu₄AlO_x and CuO/γ-Al₂O₃ after exposure to 50 ppm SO₂ at 200 °C

for 1 h were performed, as shown in Fig. 11(a). One major SO₂ desorption peak was observed for Cu₄AlO_x and CuO/γ-Al₂O₃ at around 643 and 686 °C, respectively, which can be attributed to the decomposition of sulfate species [63, 64]. The SO₂ desorption peak for CuO/γ-Al₂O₃ is much larger than that for Cu₄AlO_x, demonstrating Cu₄AlO_x is more SO₂ resistant and with less SO₂ adsorption on its surface. Fig. 11(b) shows the FTIR spectra of the fresh and pre-sulfated Cu₄AlO_x catalysts. For the pre-sulfated Cu₄AlO_x, two new bands at 1037 and 1124 cm⁻¹ were observed. According to literature [47], these bands could be attributed to the characteristic band of SO₄²⁻. It can be concluded that the formation of sulfate species on the sample is the cause of SO₂ poisoning. To identify this, the thermal stability of pre-sulfated Cu₄AlO_x was further studied by TGA. The TGA spectra in Fig. 11(c) reveal a loss of mass of the poisoned sample in three steps. Step A (26–200 °C) could be mainly assigned to the desorption of adsorbed water on the sample [65, 66]. The loss of mass at Step B (200–455 °C) was caused by the decomposition of (NH₄)₂SO₄ [46], while the loss of mass at Step C (455–700 °C) corresponds to CuSO₄. Pre-sulfated Cu₄AlO_x sample showed a weight reduction of 3.77 wt%.

The regeneration of SO₂-poisoned Cu₄AlO_x and CuO/γ-Al₂O₃ catalysts were also investigated at 200 °C, as shown in Fig. 11(d). At the first stage (section a), without SO₂, the NO_x conversion was about 91.1% and 81.8% for Cu₄AlO_x and CuO/γ-Al₂O₃, respectively. After introducing 50 ppm SO₂ (section b), the NO_x conversions for both Cu₄AlO_x and CuO/γ-Al₂O₃ were decreased, which became 78.4% and 48%, respectively. When SO₂ was cut off from the feed stream (section c), the NO_x conversion of CuO/γ-Al₂O₃ did not recover at all, suggesting that the deactivation by SO₂ is irreversible for CuO/γ-Al₂O₃. However, for Cu₄AlO_x, the NO_x conversion slightly increased from 78.4% to 80.2%.

In order to reuse the SO₂ deactivated SCR catalysts, the thermal regeneration method was normally applied. In section d of Fig. 11(d), the deactivated catalysts were calcined at 400 °C in Ar for 1 h to purge the catalyst. After purging, the catalysts were cooled down to the reaction temperature of 200 °C, and tested under the same condition as that in section a. After this treatment, the catalytic activities were somehow recovered. The NO_x conversion was increased from 80.2% to 83.4% for Cu₄AlO_x and 48.8% to 51.6% for CuO/γ-Al₂O₃, respectively (section e). However, the NO_x conversion still much lower than that in section a. These experimental results clearly indicate that Cu₄AlO_x has a better resistance to SO₂ than CuO/γ-Al₂O₃. The deactivation may result from the formation of sulfate species, which is consistent with the results of SO₂-TPD.

3.6 SO₂ and H₂O poisoning of catalysts

Water vapor is one of the main components in flue gases and often leads to catalyst deactivation by decreasing the number of available active sites. Even in dry conditions, water vapor also can destroy the catalysts since it is produced in the SCR reaction. It has been reported that the water vapor can cause a reduction in activity to some extent for both non-supported metal oxide catalysts [67, 68] and carbon based catalysts [69]. The effect of H₂O can be divided into two categories, reversible and irreversible [70]. Reversible effect come from the H₂O adsorption that competes with that of NH₃ and NO. This H₂O effect will disappear with removing. However, the hydroxyl formed by H₂O adsorption and decomposition on the surface of catalysts will lead to irreversible deactivation of catalysts. The generating hydroxyl will only be pulled off under the temperature of 252–502 °C, so this kind of deactivation cannot be removed by removing H₂O in the gas phase [70]. Therefore a comparative study was conducted to

evaluate the H₂O poisoning effect on Cu₄AlO_x and CuO/ γ -Al₂O₃ catalysts in this regard.

Fig. 12(a) shows the comparative study on the influence of 5% H₂O on the NO_x conversion of Cu₄AlO_x and CuO/ γ -Al₂O₃ catalysts at 150 and 200 °C. After introducing 5% H₂O, the NO_x conversions for both Cu₄AlO_x and CuO/ γ -Al₂O₃ began to decrease. At 200 °C, the NO_x conversion of CuO/ γ -Al₂O₃ decreased from 81.7% to 66.3%. However, for Cu₄AlO_x catalyst, its NO_x conversion was still as high as 78.3%. At lower temperature (150 °C), the NO_x conversion declined to 38.8% for Cu₄AlO_x and 23.9% for CuO/ γ -Al₂O₃, respectively. It is because of the greater affinity of water vapor with catalysts at lower temperatures. The results demonstrated that although Cu₄AlO_x was also effected by 5% H₂O, its performance is still much better than that of CuO/ γ -Al₂O₃.

It is well known that H₂O and SO₂ have a critical influence on SCR catalysts for NO_x reduction at low temperatures. Huang et al. [71] studied that the co-existence of H₂O and SO₂ resulted in an obvious decrease on V₂O₅/AC catalyst. The phenomenon was possibly caused by sulfate particles formed from H₂O and SO₂, which led to the blocking of pores and covering of catalysts surface [72]. Thus, the resistance of Cu₄AlO_x and CuO/ γ -Al₂O₃ to the co-existence of H₂O and SO₂ in the SCR reaction system was also studied at 200 °C, as shown in Fig. 12(b). At the first stage (section a), without H₂O and SO₂, the NO_x conversion was about 91.1% and 81.8% for Cu₄AlO_x and CuO/ γ -Al₂O₃, respectively. After adding 5% H₂O (section b), the NO_x conversion of Cu₄AlO_x and CuO/ γ -Al₂O₃ decreased to 78.3% and 66.3%, respectively. After adding 5% H₂O and 50 ppm SO₂ (section c) to the system simultaneously, the synergistic deactivating effect of H₂O and SO₂ further inhibited the performance of both catalysts. However, Cu₄AlO_x showed much better performance than

CuO/ γ -Al₂O₃ even with both H₂O and SO₂. For Cu₄AlO_x, the NO_x conversion was still 67.6% after 6 h. While for CuO/ γ -Al₂O₃, the NO_x conversion was only 37.7% after 6 h. In addition, once SO₂ and H₂O were removed (section d), the NO_x conversion for Cu₄AlO_x recovered to 73.3%, but only 49.3% for CuO/ γ -Al₂O₃. This data suggests that our newly developed Cu₄AlO_x catalyst also possesses much better resistance to the co-existence of H₂O and SO₂ than the conventional CuO/ γ -Al₂O₃ catalyst.

4. Conclusions

In this work, the highly dispersed Cu₄AlO_x mixed oxide was found to be an NH₃-SCR catalyst with high thermal stability, excellent low-temperature catalytic De-NO_x activity, and improved alkali metal and SO₂ resistance. The highly dispersed Cu₄AlO_x catalyst was synthesized from calcination of a high surface area AMO-Cu₄Al-CO₃ LDH precursor. XRD, FTIR, SEM and TEM analyses demonstrated the successful synthesis of a series of flower-like LDHs, which are good precursors for the fabrication of highly dispersed Cu_yAlO_x ($y = 2-5$) mixed oxide catalysts. The best catalyst Cu₄AlO_x showed much higher catalytic activity and thermal stability than the control catalyst CuO/ γ -Al₂O₃. At 200 °C, the NO_x conversion of Cu₄AlO_x and CuO/ γ -Al₂O₃ was 91.1% and 81.8%, which decreased to 84.7% and 57.5% after being calcined at 700 °C, respectively. XRD and HR-TEM analyses indicated that the Cu₄AlO_x catalyst mainly contains well dispersed CuO nanoparticles with an average particle size of ~10 nm, while the CuO/ γ -Al₂O₃ catalyst contains CuAl₂O₄ nanoparticles with an average particle size of ~20 nm. Although the Cu₄AlO_x catalyst could be poisoned to some extent by both K and Na, the poisoned samples still showed much higher NO_x conversions (74.3–74.7%) than those of poisoned CuO/ γ -Al₂O₃ catalysts (68.6–69.3%), and the NO_x conversion can be recovered to

77.9% and 79.9% after regeneration. NH_3 -TPD and H_2 -TPR analyses revealed that both the surface acid sites and surface redox property of Cu_4AlO_x catalyst were much less influenced by K and Na than $\text{CuO}/\gamma\text{-Al}_2\text{O}_3$ catalyst. After long-term running with 50 ppm SO_2 for 6 h, the NO_x conversion of Cu_4AlO_x catalyst only decreased by 5%, which was much less than that of $\text{CuO}/\gamma\text{-Al}_2\text{O}_3$ (12%). We also demonstrated that our newly developed Cu_4AlO_x catalyst possesses much better resistance to the co-existence of H_2O and SO_2 than the conventional $\text{CuO}/\gamma\text{-Al}_2\text{O}_3$ catalyst. In all, the newly obtained Cu_4AlO_x catalyst has shown much better performance than the conventional supported catalyst and is promising as low-temperature NH_3 -SCR catalyst for NO_x control from the flue gases of MSW incinerators.

Acknowledgements

This work was supported by the Fundamental Research Funds for the Central Universities (2016ZCQ03), Beijing Excellent Young Scholar (2015000026833ZK11), and the National Natural Science Foundation of China (51622801, 51572029, and 51308045).

References

- [1] Y. Jiang, X. Gao, Y. Zhang, W. Wu, H. Song, Z. Luo, K. Cen, J. Hazard. Mater. 274 (2014) 270-278.
- [2] H.-H. Tseng, C.-Y. Lu, F.-Y. Chang, M.-Y. Wey, H.-T. Cheng, Chem. Eng. J. 169 (2011) 135-143.
- [3] X. Gao, X. Du, Y. Fu, J. Mao, Z. Luo, M. Ni, K. Cen, Catal. Today 175 (2011) 625-630.
- [4] L. Lisi, G. Lasorella, S. Malloggi, G. Russo, Appl. Catal. B: Environ. 50 (2004) 251-258.
- [5] S. Zhang, Q. Zhong, J. Mol. Catal. A: Chem. 373 (2013) 108-113.
- [6] S. Djerad, M. Crocoll, S. Kureti, L. Tifouti, W. Weisweiler, Catal. Today 113 (2006) 208-214.
- [7] P. Cloirec Le, Rev. Environ. Sci. Biotechnol. 11 (2012) 381-392.
- [8] J.P. Dunn, P.R. Koppula, H.G. Stenger, I.E. Wachs, Appl. Catal. B: Environ. 19 (1998) 103-117.

- [9] H. Tounsi, S. Djemal, C. Petitto, G. Delahay, *Appl. Catal. B: Environ.* 107 (2011) 158-163.
- [10] B. Thirupathi, P.G. Smirniotis, *J. Catal.* 288 (2012) 74-83.
- [11] Y. Peng, J. Li, W. Si, J. Luo, Y. Wang, J. Fu, X. Li, J. Crittenden, J. Hao, *Appl. Catal. B: Environ.* 168 (2015) 195-202.
- [12] Y. Peng, J. Li, X. Huang, X. Li, W. Su, X. Sun, D. Wang, J. Hao, *Environ. Sci. Technol.* 48 (2014) 4515-4520.
- [13] R. Moreno-Tost, J. Santamaría-González, E. Rodríguez-Castellón, A. Jiménez-López, *Appl. Catal. B: Environ.* 52 (2004) 241-249.
- [14] L. Xie, F. Liu, X. Shi, F.-S. Xiao, H. He, *Appl. Catal. B: Environ.* 179 (2015) 206-212.
- [15] L. Ma, Y. Cheng, G. Cavataio, R.W. McCabe, L. Fu, J. Li, *Appl. Catal. B: Environ.* 156 (2014) 428-437.
- [16] F. Liu, W. Shan, Z. Lian, L. Xie, W. Yang, H. He, *Catal. Sci. Technol.* 3 (2013) 2699-2707.
- [17] Q. Liu, Z. Liu, J. Su, *Catal. Today* 158 (2010) 370-376.
- [18] J. Su, Q. Liu, Z. Liu, Z. Huang, *Ind. Eng. Chem. Res.* 47 (2008) 4295-4301.
- [19] J.W. Choung, I.-S. Nam, *Appl. Catal. B: Environ.* 64 (2006) 42-50.
- [20] J.W. Choung, I.-S. Nam, *Appl. Catal. A: Gen.* 312 (2006) 165-174.
- [21] G.G. Park, H.J. Chae, I.-S. Nam, J.W. Choung, K.H. Choi, *Microporous Mesoporous Mater.* 48 (2001) 337-343.
- [22] H. Chang, X. Chen, J. Li, L. Ma, C. Wang, C. Liu, J.W. Schwank, J. Hao, *Environ. Sci. Technol.* 47 (2013) 5294-5301.
- [23] Z. Si, D. Weng, X. Wu, J. Li, G. Li, *J. Catal.* 271 (2010) 43-51.
- [24] D. Pietrogiacomì, D. Sannino, A. Magliano, P. Ciambelli, S. Tuti, V. Indovina, *Appl. Catal. B: Environ.* 36 (2002) 217-230.
- [25] A. Caballero, J.J. Morales, A.M. Cordon, J.P. Holgado, J.P. Espinos, A.R. Gonzalez-Elipse, *J. Catal.* 235 (2005) 295-301.
- [26] D. Pietrogiacomì, A. Magliano, D. Sannino, M.C. Campa, P. Ciambelli, V. Indovina, *Appl. Catal. B: Environ.* 60 (2005) 83-92.
- [27] S. Suárez, J.A. Martín, M. Yates, P. Avila, J. Blanco, *J. Catal.* 229 (2005) 227-236.
- [28] J.A. Sullivan, J.A. Doherty, *Appl. Catal. B: Environ.* 55 (2005) 185-194.
- [29] G. Ramis, L. Yi, G. Busca, M. Turco, E. Kotur, R.J. Willey, *J. Catal.* 157 (1995) 523-535.
- [30] X. Jiang, G. Ding, L. Lou, Y. Chen, X. Zheng, *J. Mol. Catal. A: Chem.* 218 (2004) 187-195.
- [31] G. Centi, S. Perathoner, *Appl. Catal. A: Gen.* 132 (1995) 179-259.
- [32] Q. Wang, X. Zhang, J. Zhu, Z. Guo, D. O'Hare, *Chem. Commun.* 48 (2012) 7450-7452.
- [33] Q. Wang, D. O'Hare, *Chem. Commun.* 49 (2013) 6301-6303.
- [34] Q. Wang, J.P. Undrell, Y. Gao, G. Cai, J.-C. Buffet, C.A. Wilkie, D. O'Hare, *Macromolecules* 46 (2013) 6145-6150.
- [35] Y. Zhao, G. Chen, T. Bian, C. Zhou, G.I.N. Waterhouse, L.-Z. Wu, C.-H. Tung, L.J. Smith, D. O'Hare, T. Zhang, *Adv. Mater.* 27 (2015) 7824-7831.
- [36] Y. Zhao, B. Zhao, J. Liu, G. Chen, R. Gao, S. Yao, M. Li, Q. Zhang, L. Gu, J. Xie, X. Wen, L.-Z. Wu, C.-H. Tung, D. Ma, T. Zhang, *Angew. Chem. Int. Ed.* 55 (2016) 4215-4219.
- [37] Q. Wang, D. O'Hare, *Chem. Rev.* 7 (2012) 4124-4155.

- [38] Q. Wang, S.V.Y. Tang, E. Lester, D. O'Hare, *Nanoscale* 5 (2013) 114-117.
- [39] Y. Zhao, Q. Wang, T. Bian, H. Yu, H. Fan, C. Zhou, L.-Z. Wu, C.-H. Tung, D. O'Hare, T. Zhang, *Nanoscale* 7 (2015) 7168-7173.
- [40] Z. Zhang, J. Wang, L. Huang, Y. Gao, A. Umar, Z. Huang, Q. Wang, *Sci. Adv. Mater.* 6 (2014) 1154-1159.
- [41] S. Kannan, V. Rives, H. Knözinger, *J. Solid State Chem.* 177 (2004) 319-331.
- [42] J.M. Gatica, H. Vidal, *J. Hazard. Mater.* 181 (2010) 9-18.
- [43] Q. Wang, Z. Wu, H.H. Tay, L. Chen, Y. Liu, J. Chang, Z. Zhong, J. Luo, A. Borgna, *Catal. Today* 164 (2011) 198-203.
- [44] J. Wang, Z. Lei, H. Qin, L. Zhang, F. Li, *Ind. Eng. Chem. Res.* 50 (2011) 7120-7128.
- [45] C.J. Wang, D. O'Hare, *J. Mater. Chem.* 22 (2012) 23064-23070.
- [46] P. Zhang, G. Qian, Z.P. Xu, H. Shi, X. Ruan, J. Yang, R.L. Frost, *J. Colloid Interface Sci.* 367 (2012) 264-271.
- [47] P. Zhang, G. Qian, H. Cheng, J. Yang, H. Shi, R.L. Frost, *Spectrochim. Acta Part A* 79 (2011) 548-553.
- [48] G. Centi, S. Perathoner, D. Biglino, E. Giamello, *J. Catal.* 151 (1995) 75-92.
- [49] G. Centi, S. Perathoner, *J. Catal.* 152 (1995) 93-102.
- [50] F.H. Chung, *J. Appl. Cryst.* 7 (1974) 526-531.
- [51] O. Omotoso, D.K. McCarty, S. Hillier, R. Kleeberg, *Clays and Clay Minerals* 54 (2006) 748-760.
- [52] A. Gervasini, M. Manzoli, G. Martra, A. Ponti, N. Ravasio, L. Sordelli, F. Zaccheria, *J. Phys. Chem. B* 110 (2006) 7851-7861.
- [53] R. Khodayari, C.U.I. Odenbrand, *Appl. Catal. B: Environ.* 30 (2001) 87-99.
- [54] L. Chen, J. Li, M. Ge, *Chem. Eng. J.* 170 (2011) 531-537.
- [55] Q. Wan, L. Duan, J. Li, L. Chen, K. He, J. Hao, *Catal. Today* 175 (2011) 189-195.
- [56] B. Shen, Y. Yao, J. Chen, X. Zhang, *Microporous Mesoporous Mater.* 180 (2013) 262-269.
- [57] M. Fu, C. Li, P. Lu, L. Qu, M. Zhang, Y. Zhou, M. Yu, Y. Fang, *Catal. Sci. Technol.* 4 (2014) 14-25.
- [58] D. Yuan, X. Li, Q. Zhao, J. Zhao, S. Liu, M. Tadé, *Appl. Catal. A: Gen.* 451 (2013) 176-183.
- [59] C. Sun, J. Zhu, Y. Lv, L. Qi, B. Liu, F. Gao, K. Sun, L. Dong, Y. Chen, *Appl. Catal. B: Environ.* 103 (2011) 206-220.
- [60] D. Yuan, X. Li, Q. Zhao, J. Zhao, M. Tade, S. Liu, *J. Catal.* 309 (2014) 268-279.
- [61] W. Xu, H. He, Y. Yu, *J. Phys. Chem. C* 113 (2009) 4426-4432.
- [62] Y. Xiong, C. Tang, X. Yao, L. Zhang, L. Li, X. Wang, Y. Deng, F. Gao, L. Dong, *Appl. Catal. A: Gen.* 495 (2015) 206-216.
- [63] M. Waqif, O. Saur, J.C. Lavalley, S. Perathoner, G. Centi, *J. Phys. Chem.* 95 (1991) 4051-4058.
- [64] K.S. Yoo, S.D. Kim, S.B. Park, *Ind. Eng. Chem. Res.* 33 (1994) 1786-1791.
- [65] D.W. Kwon, K.B. Nam, S.C. Hong, *Appl. Catal. B: Environ.* 166-167 (2015) 37-44.

- [66] L. Zhang, L. Li, Y. Cao, X. Yao, C. Ge, F. Gao, Y. Deng, C. Tang, L. Dong, *Appl. Catal. B: Environ.* 165 (2015) 589-598.
- [67] G. Qi, R.T. Yang, R. Chang, *Appl. Catal. B: Environ.* 51 (2004) 93-106.
- [68] R. Moreno-Tost, E.R. Castellon, A. Jimenez-Lopez, *J. Mol. Catal. A: Chem.* 248 (2006) 126-134.
- [69] M.E. Gálvez, M.J. Lázaro, R. Moliner, *Catal. Today* 102-103 (2005) 142-147.
- [70] J. Li, H. Chang, L. Ma, J. Hao, R.T. Yang, *Catal. Today* 175 (2011) 147-156.
- [71] Z. Huang, Z. Zhu, Z. Liu, *Appl. Catal. B: Environ.* 39 (2002) 361-368.
- [72] X. Lu, C. Song, S. Jia, Z. Tong, X. Tang, Y. Teng, *Chem. Eng. J.* 260 (2015) 776-784.

Table 1. Specific surface area, pore size, and pore volume of Cu_2AlO_x , Cu_3AlO_x , Cu_4AlO_x , and Cu_5AlO_x .

Samples	BET SSA (m^2/g)	BJH pore size (\AA)	BJH pore volume (cm^3/g)
Cu_2AlO_x	93.0	228.3	0.6
Cu_3AlO_x	102.1	218.1	0.7
Cu_4AlO_x	108.4	206	0.92
Cu_5AlO_x	100.3	169.7	0.85

Table 2. The mole ratio of active species calculated by a normalize RIR method.

Samples	Calcination temperature (°C)	Chemical components	
		CuO (%)	CuAl ₂ O ₄ (%)
Cu ₄ AlO _x	400	100	0
	500	99.2	0.8
	600	97.5	2.5
	700	94.9	5.1
CuO/ γ -Al ₂ O ₃	400	58	42
	500	54	46
	600	40.8	59.2
	700	27.7	72.3

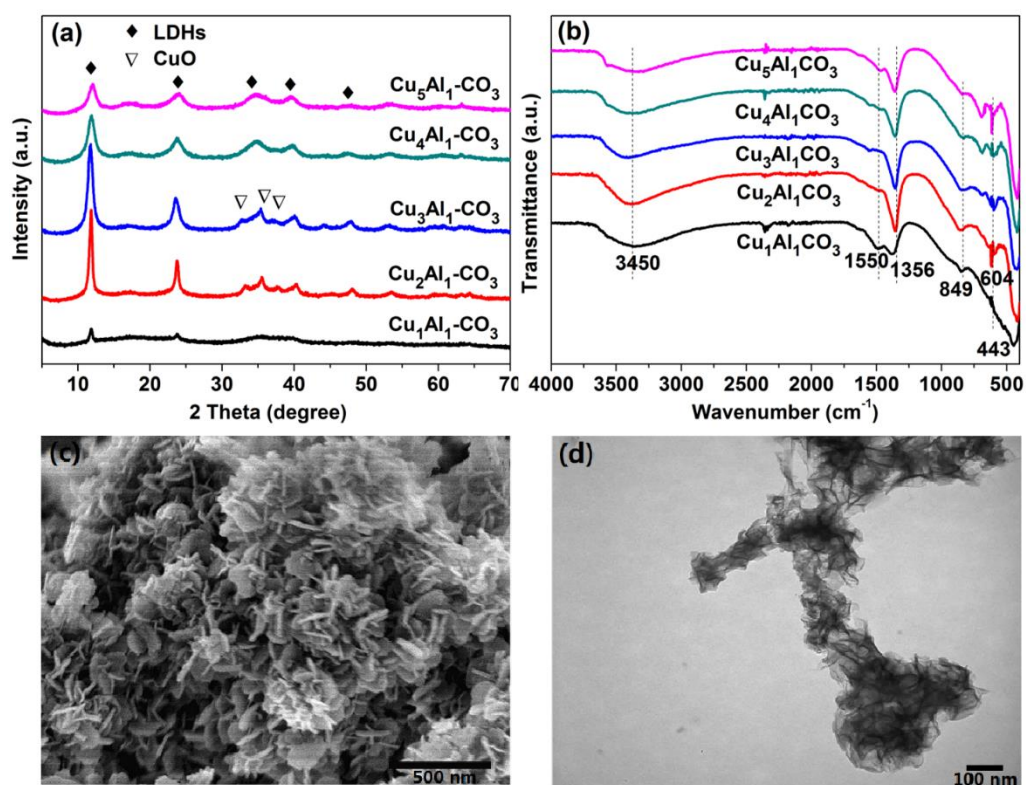


Fig. 1. (a) XRD patterns and (b) FTIR spectra of AMO-Cu-Al-CO₃ LDHs synthesized with different Cu/Al ratios, (c) SEM and (d) TEM image of AMO-Cu₄Al-CO₃ LDH.

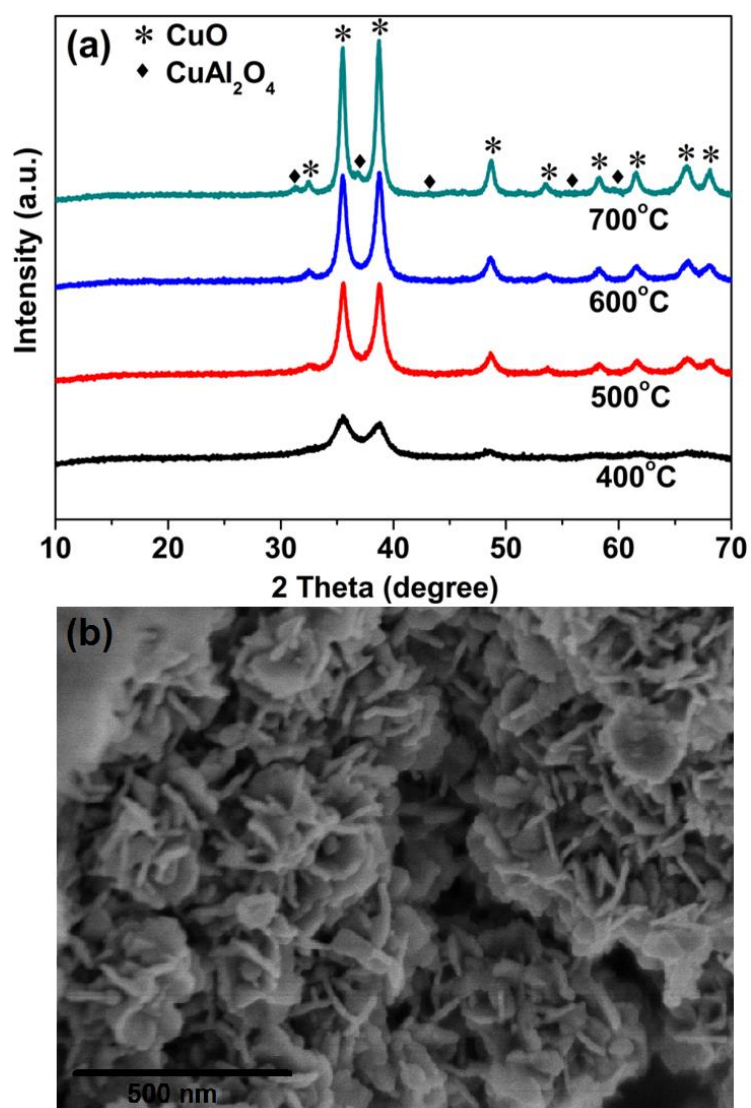


Fig. 2. (a) The XRD patterns of Cu_4AlO_x calcined at different temperatures (400, 500, 600, and 700 °C), and (b) The SEM image of Cu_4AlO_x calcined at 400 °C.

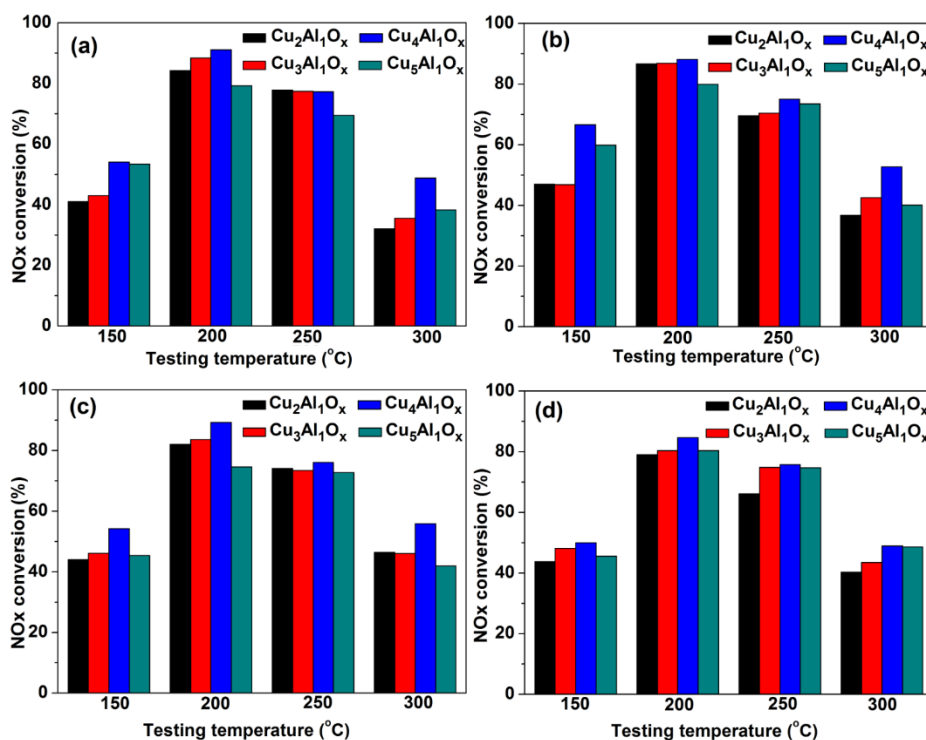


Fig. 3. The influence of Cu/Al ratio (2, 3, 4, and 5), calcination temperature (400, 500, 600, and 700 °C), and operating temperature (150, 200, 250, and 300 °C) on the activity of Cu-Al mixed oxide catalysts. All samples were calcined at (a) 400 °C, (b) 500 °C, (c) 600 °C, and (d) 700 °C. Reaction conditions: $[\text{NO}_x] = [\text{NH}_3] = 500$ ppm, $[\text{O}_2] = 5\%$, balance Ar, total flow rate = 200 mL/min, catalyst 0.15 g.

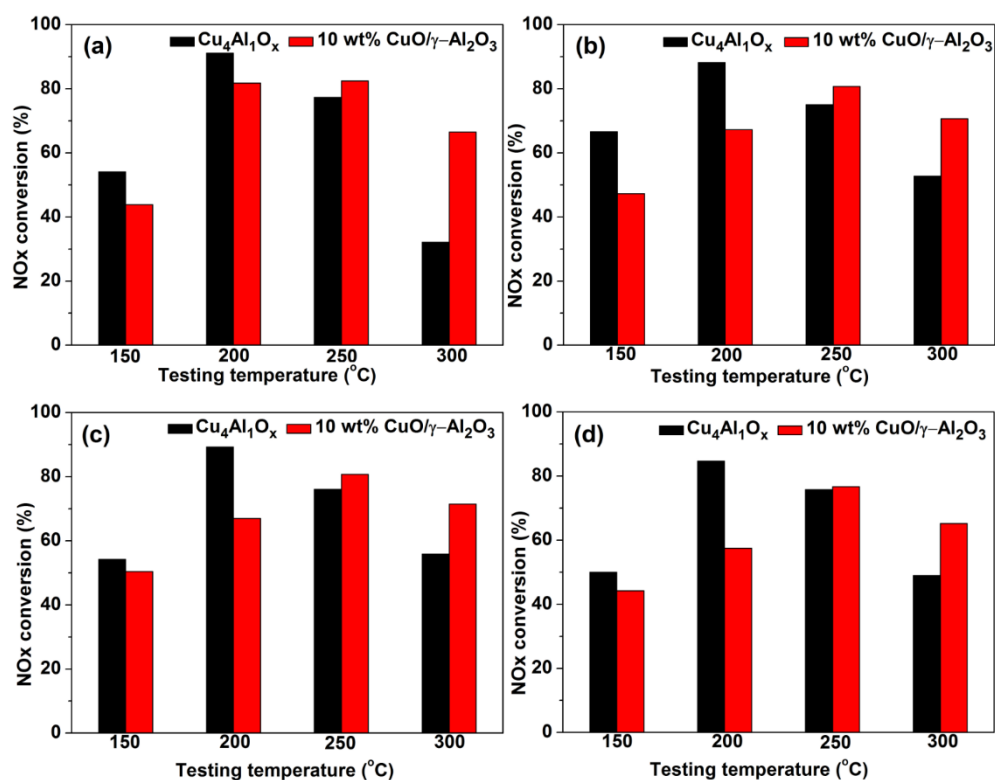


Fig. 4. The influences of calcination and testing temperatures on the NO_x conversion of $\text{Cu}_4\text{Al}_1\text{O}_x$ and $\text{CuO}/\gamma\text{-Al}_2\text{O}_3$. All samples were calcined at (a) 400 °C, (b) 500 °C, (c) 600 °C, and (d) 700 °C. Reaction conditions: $[\text{NO}_x] = [\text{NH}_3] = 500$ ppm, $[\text{O}_2] = 5\%$, balance Ar, total flow rate = 200 mL/min, catalyst 0.15 g.

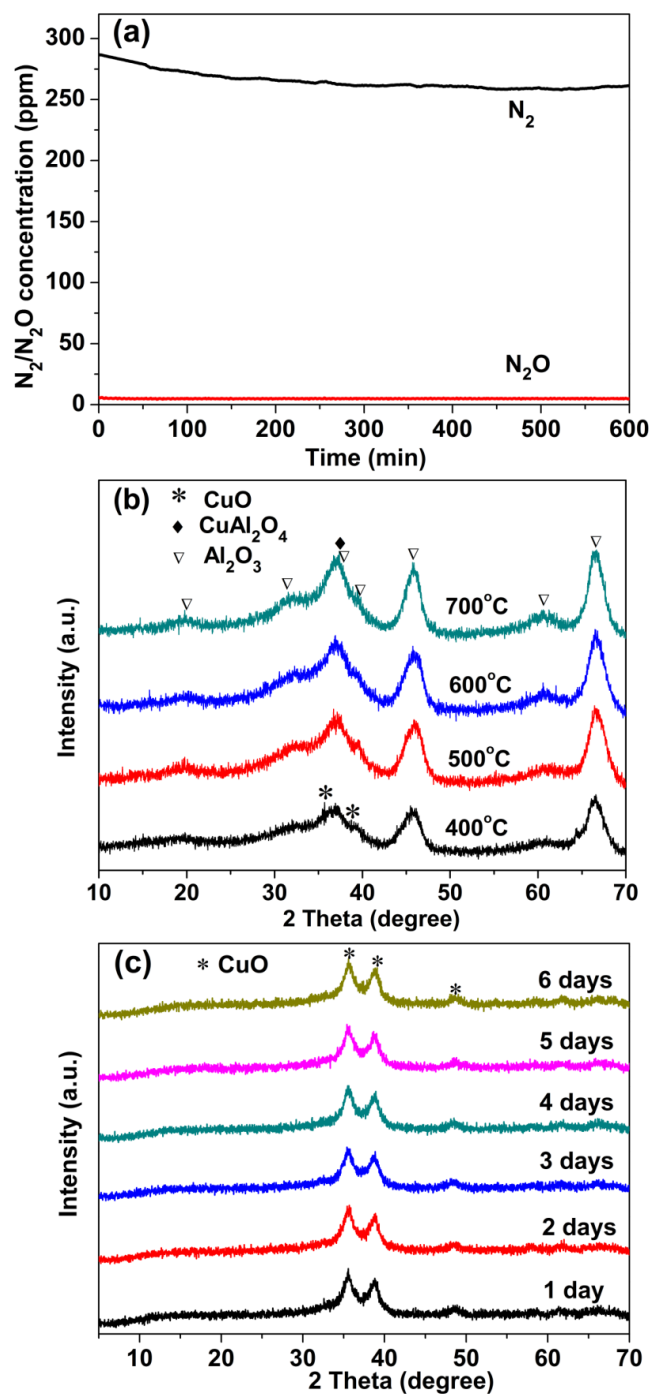


Fig. 5. (a) The N_2O and N_2 evolutions in the outlet for the Cu_4AlO_x catalyst tested at 200 °C, (b) The XRD patterns of $CuO/\gamma-Al_2O_3$ calcined at different temperatures (400, 500, 600, and 700 °C), and (c) The XRD patterns of Cu_4AlO_x LDO after being exposed to ambient atmosphere for different days. Reaction conditions: $[NO_x] = [NH_3] = 500$ ppm, $[O_2] = 5\%$, balance Ar, total flow rate 200 mL/min, catalyst 0.15 g.

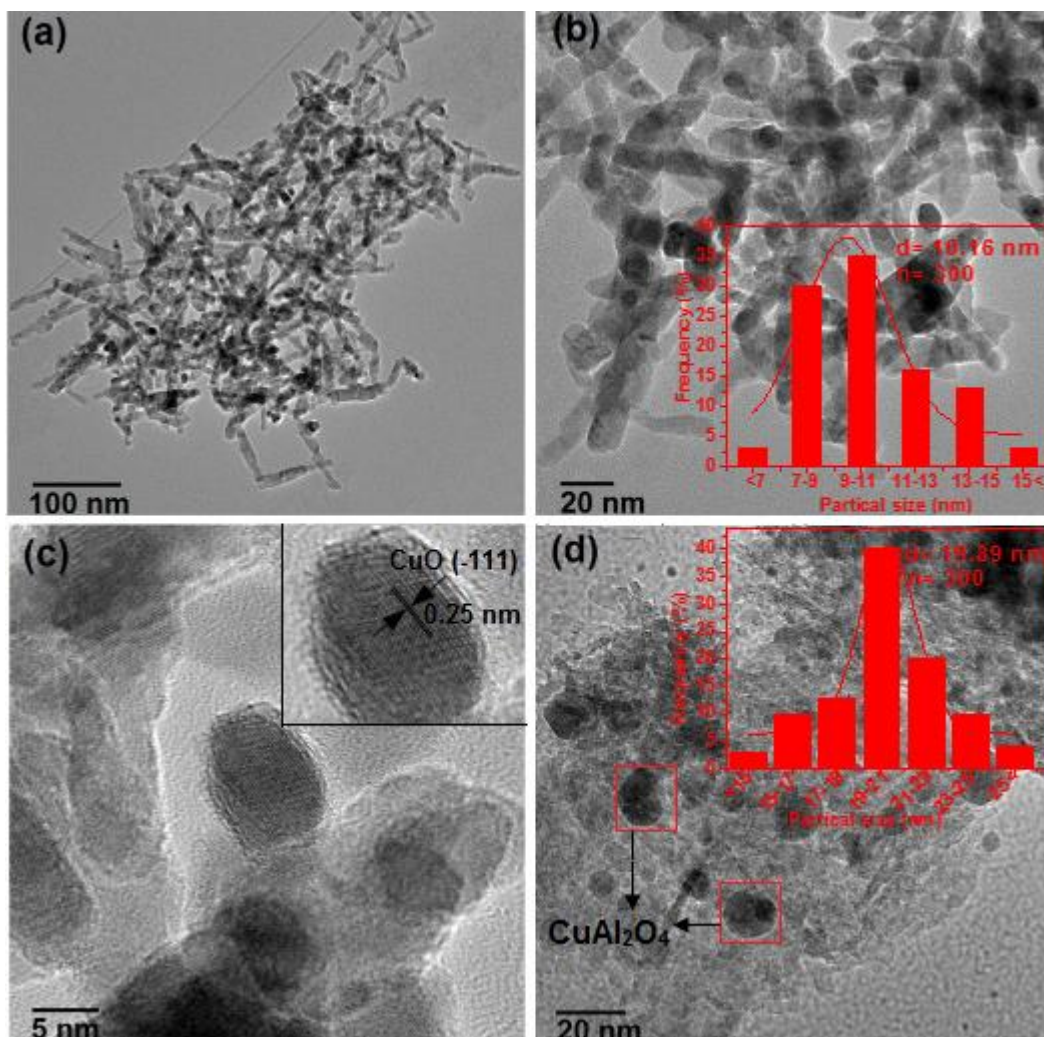


Fig. 6. The HR-TEM images of (a, b, c) Cu_4AlO_x and (d) $\text{CuO}/\gamma\text{-Al}_2\text{O}_3$ calcined at 400 °C. The inset shows the particle size distribution of CuO in Cu_4AlO_x catalyst and the particle size distribution of CuAl_2O_4 in $\text{CuO}/\gamma\text{-Al}_2\text{O}_3$ catalyst.

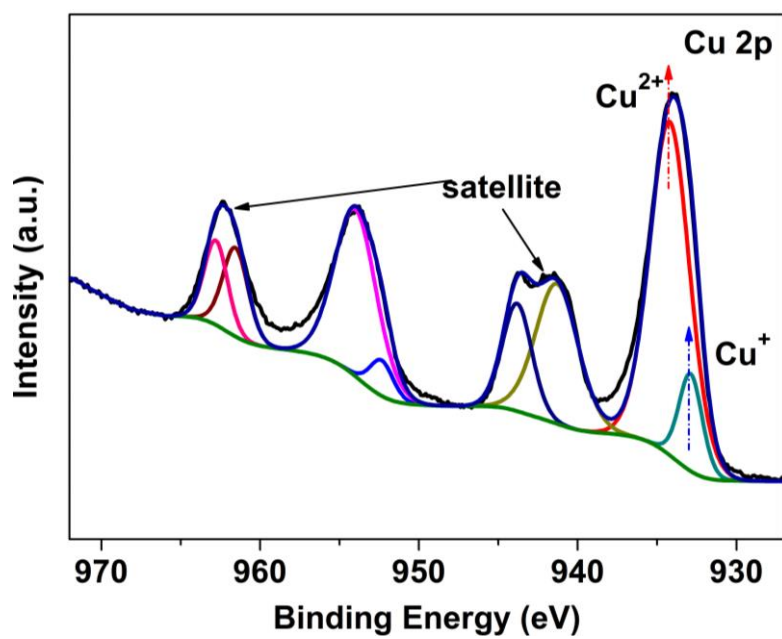


Fig. 7. XPS result of Cu 2p in the calcined Cu_4AlO_x catalyst.

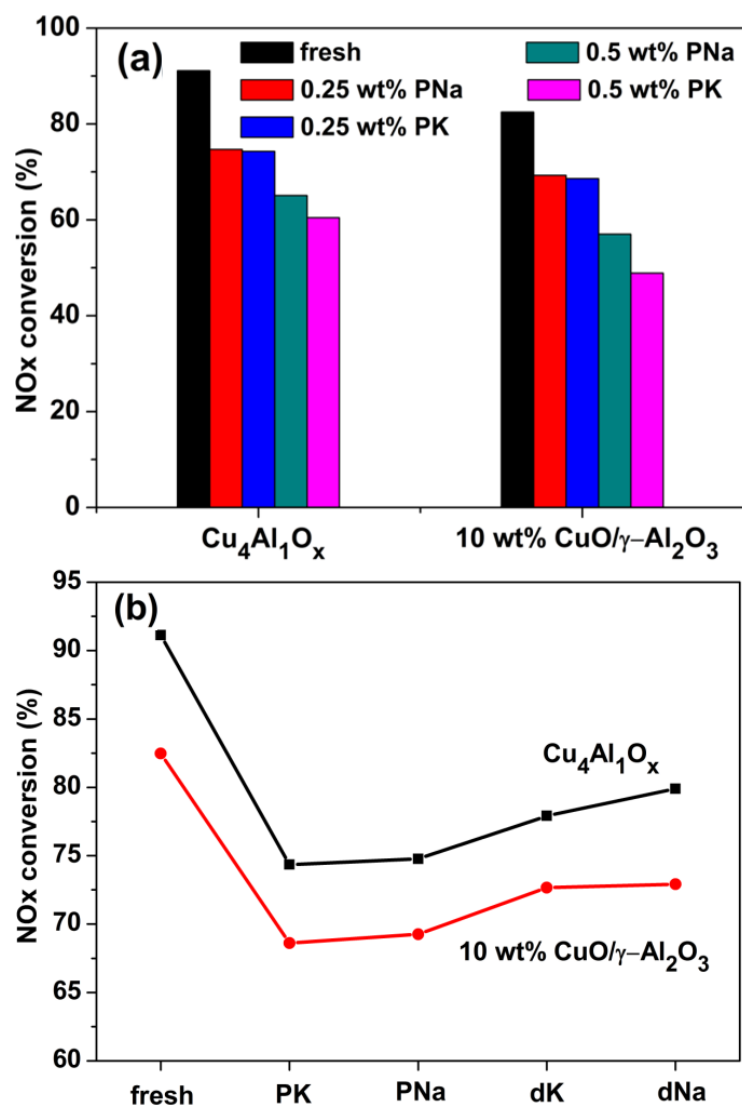


Fig. 8. (a) The NO_x conversions of fresh, 0.25 wt% K or Na, and 0.5 wt% K or Na poisoned Cu₄AlO_x and CuO/γ-Al₂O₃ catalysts at 200 °C, and (b) The NO_x conversions of fresh, 0.25 wt% K or Na poisoned, and regenerated Cu₄AlO_x and CuO/γ-Al₂O₃ catalysts. Reaction conditions: [NO_x] = [NH₃] = 500 ppm, [O₂] = 5%, balance Ar, total flow rate 200 mL/min, catalyst 0.15 g. PK and PNa represent the K and Na poisoned samples, and dK and dNa represent the corresponding regenerated samples.

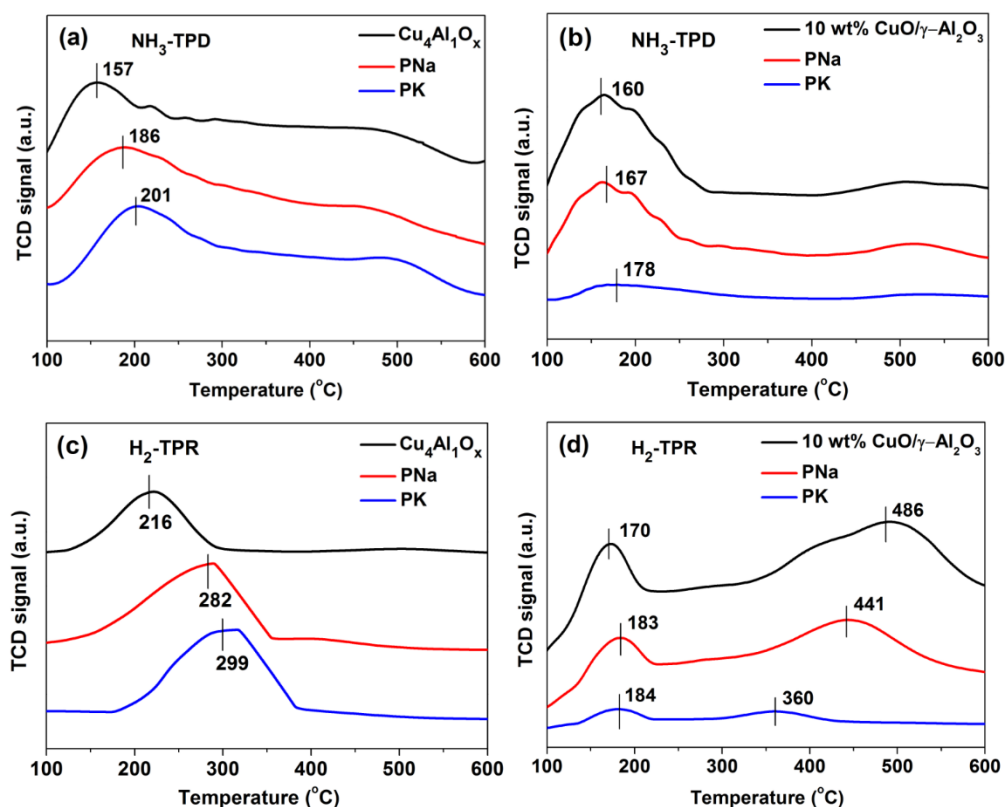


Fig. 9. NH₃-TPD and H₂-TPR profiles of fresh, and K and Na-poisoned Cu₄AlO_x and CuO/γ-Al₂O₃ catalysts, (a) NH₃-TPD of Cu₄AlO_x, (b) NH₃-TPD of CuO/γ-Al₂O₃, (c) H₂-TPR of Cu₄AlO_x, and (d) H₂-TPR of CuO/γ-Al₂O₃. PK and PNa represent the K and Na poisoned samples.

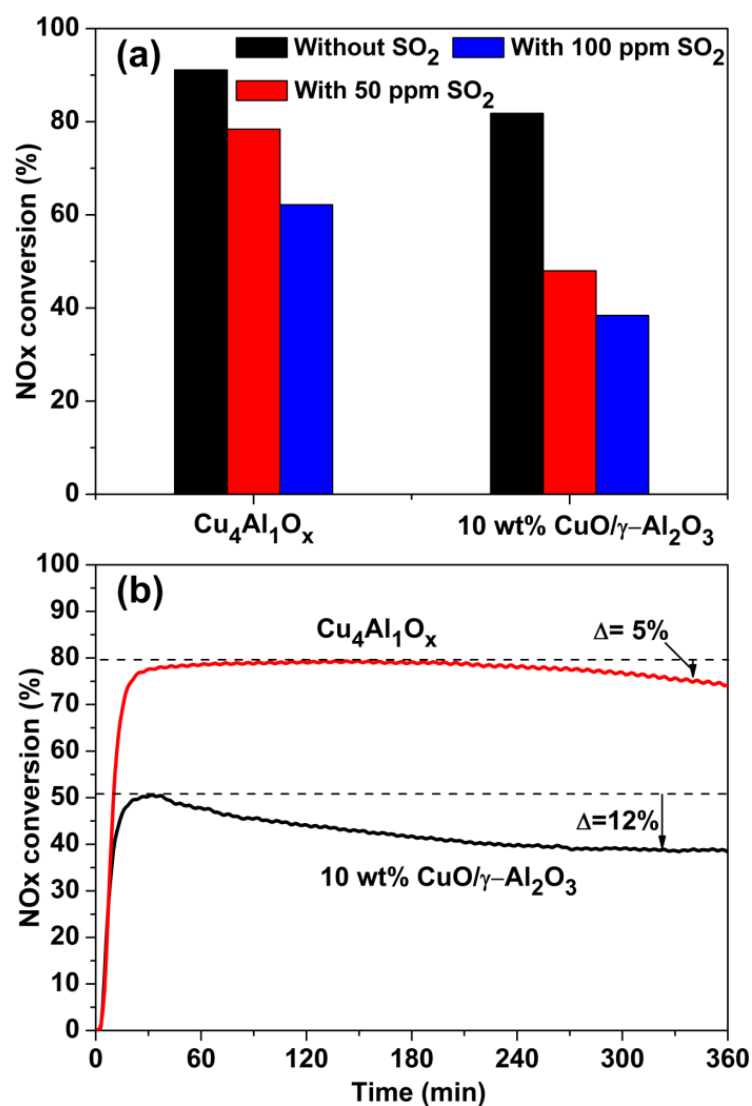


Fig. 10. (a) The comparison of NO_x conversions of Cu₄AlO_x and CuO/γ-Al₂O₃ catalysts with and without 50 or 100 ppm SO₂ at 200 °C, and (b) Long-term isothermal NO_x conversion of Cu₄AlO_x and CuO/γ-Al₂O₃ catalysts in the presence of 50 ppm SO₂ at 200 °C. Reaction conditions: [NO_x] = [NH₃] = 500 ppm, [O₂] = 5%, [SO₂] = 50 ppm, balance Ar, total flow rate 200 mL/min, catalyst 0.15 g.

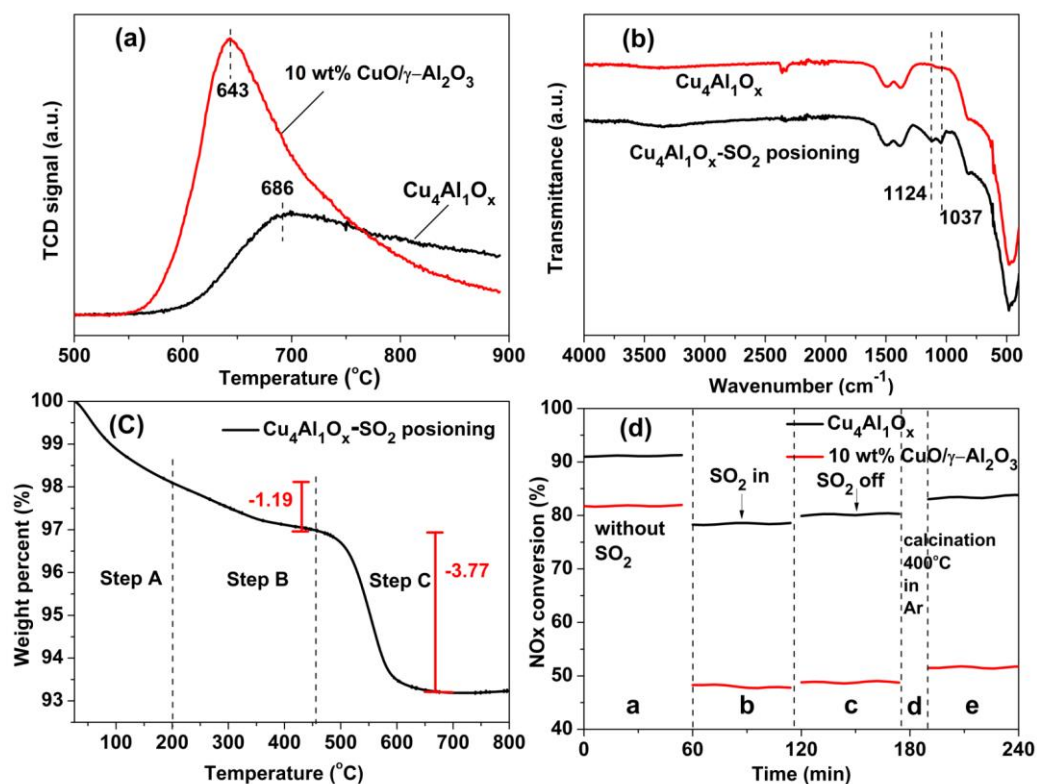


Fig. 11. (a) SO_2 -TPD of pre-sulfated Cu_4AlO_x and $\text{CuO}/\gamma\text{-Al}_2\text{O}_3$ catalysts, (b) FTIR spectra of Cu_4AlO_x and pre-sulfated Cu_4AlO_x , (c) TGA curve of pre-sulfated Cu_4AlO_x , and (d) The influence of SO_2 addition and the thermal regeneration on the NO_x conversion of Cu_4AlO_x and $\text{CuO}/\gamma\text{-Al}_2\text{O}_3$ catalysts. Reaction conditions: $[\text{NO}_x] = [\text{NH}_3] = 500 \text{ ppm}$, $[\text{O}_2] = 5\%$, $[\text{H}_2\text{O}] = 5\%$, $[\text{SO}_2] = 50 \text{ ppm}$, balance Ar, total flow rate = 200 mL/min , catalyst 0.15 g .

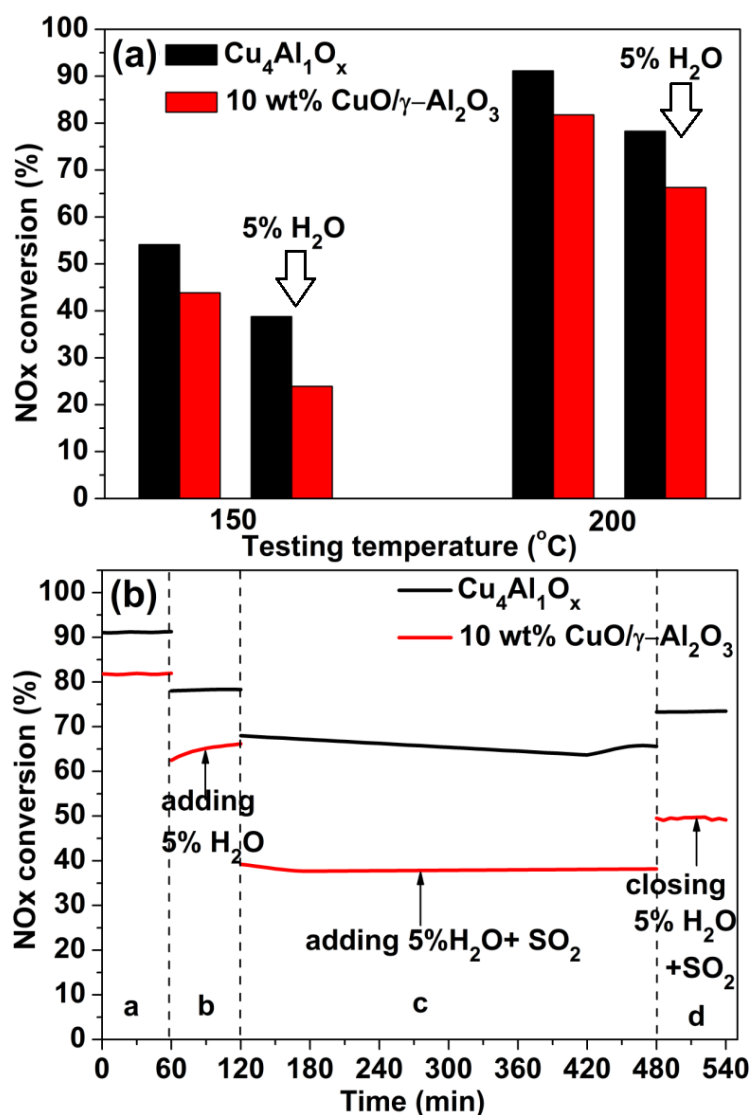


Fig. 12. (a) The influence of 5% H₂O on the NO_x conversion of Cu₄AlO_x and CuO/γ-Al₂O₃ catalysts at 150 and 200 °C, and (b) The influence of 5% H₂O and 50 ppm SO₂ addition on the NO_x conversion of Cu₄AlO_x and CuO/γ-Al₂O₃ catalysts at 200 °C. Reaction conditions: [NO_x] = [NH₃] = 500 ppm, [O₂] = 5%, [H₂O] = 5%, [SO₂] = 50 ppm, balance Ar, total flow rate = 200 mL/min, catalyst 0.15 g.